Relationship between structure and performance of a novel highly dispersed MnO$_x$ on Co-Al layered double oxide for low temperature NH$_3$-SCR

Ruihua Wang[a,1], Zhifei Hao[a,1], Yi Li[b], Guoquan Liu[a], He Zhang[a], Haitao Wang[a], Yuguo Xia[c], Sihui Zhan[a,*]

[a] MOE Key Laboratory of Pollution Processes and Environmental Criteria, Tianjin Key Laboratory of Environmental Remediation and Pollution Control, College of Environmental Science and Engineering, Tianjin Key Lab for Rare Earth Materials and Applications, Centre for Rare Earth and Inorganic Functional Materials, Nankai University, Tianjin 300350, PR China
[b] Department of Chemistry, Tianjin University, Tianjin 300072, PR China
[c] School of Chemistry & Chemical Engineering, National Engineering Research Center for Colloidal Materials, Shandong University, Jinan 250100, PR China

ABSTRACT

A series of novel highly dispersed MnO$_x$ on Co-Al layered double oxide catalysts were fabricated for the low temperature NH$_3$-SCR reaction. The Mn(0.25)/LDO exhibited outstanding catalytic performance with a unique multi-layered structure, which could achieve approximately 100% conversion of NO$_x$ in the range of 150–300 °C with a GHSV of 40,000 h^{-1}, as well as excellent H$_2$O or SO$_2$ tolerance and thermal stability. Various characterized techniques were applied to investigate the structural-activity relationship in the SCR reaction. The relative results indicated that the manganese addition could increase the quantity of Mn^{4+}, surface adsorbed oxygen species, reducibility and ammonia adsorption capacity. Meanwhile, this strong interaction between Co-Al LDO and highly dispersed manganese species could significantly increase the positive charge density around Mn cations (Lewis acid sites) based on DFT calculated and in situ DRIFTS. Furthermore, it is proved that the NH$_3$-SCR reaction over Mn(x)/LDO mainly follow E-R reaction pathway.

1. Introduction

Currently, air quality has been a focus of attention in the public. Concerning the poor air quality, the nitrogen oxide (NO$_x$) is one of the crucial contributors, which has caused a series of environmental issues, such as photochemical smog, haze and acid rain [1]. In general, automobile exhaust and fossil fuel combustion are the main sources of nitrogen oxides. Selective catalytic reduction (SCR) of NO with NH$_3$ has been widely considered the most effective technology for the removal of NO$_x$ [2–6]. As we all know, the operating temperature window of the NH$_3$-SCR can be divided into three types: low-temperature, medium-temperature and high-temperature. The low-temperature operating window corresponds to 100–300 °C [6]. Recently, V$_2$O$_5$-WO$_3$/TiO$_2$ and V$_2$O$_5$-MoO$_3$/TiO$_2$ show splendid SCR reactive activity, which possess desirable tolerance of SO$_2$ and high catalytic performance from 300 °C to 400 °C. However, there are some drawbacks, such as narrow work temperature window, poor N$_2$ selectivity and toxicity of vanadium [7]. Therefore, there is still a space to make a progress on the low-temperature deNO$_x$ performance of catalysts.

So far, the abundant investigations have been carried out, and have made a great development on the low-temperature NH$_3$-SCR catalysts. As reported, transition metal elements show a great potential in NH$_3$-SCR reaction [8,9]. Among the transition metal elements, manganese element exhibits outstanding low-temperature catalytic activity, and has been widely explored [10,11]. Hu et al. reported Mn-doped Co$_3$O$_4$ for the NH$_3$-SCR reaction and proposed the reaction mechanism [12]. The Co$_{0.2}$Ce$_{0.35}$Mn$_{0.45}$Ti$_{10}$ oxides also displayed a broad temperature window (180–390 °C) by the sol-gel method [13]. Some researchers dispersed active species on carriers to improve the SCR activity [14,15]. Generally, the loaded supports contain Al$_2$O$_3$, TiO$_2$, carbon materials and so on. It is demonstrated that the superior low-temperature catalytic activity has been displayed for these catalysts by the interaction between the active species and supports.

Layered double hydroxides (LDH) are a class of ionic plate like compounds and possess positively charged brucite-like layers, anions and solvation molecules existed in the interlayer region [16]. The highly dispersed layered double oxide (LDO) can be obtained by the calcination of LDH. What's more, LDO have been highly involved in the

---

field of NH_3-SCR. Wu et al. studied the SCR performance of Mn-Co-Al LDO [17]. Wang et al. investigated the reactive activity of different kinds of LDO, and related results demonstrated layered double oxides exhibited better performance than the catalysts by conventional synthetic method [18,19]. Meanwhile, the cation exchange existed in metal ions and LDH was reported, and further exploration showed that the exchange was preferable under alkaline condition [20,21]. In addition, the lamellar structure of the layered double oxides contributes to a large specific surface area, providing more attachment sites for active species. Inspired by those points, we took the Co-Al LDH as the precursors and synthesized the target catalysts (Mn(x)/LDO) by conventional impregnation.

In this work, we report a novel highly dispersed MnO_x on Co-Al layered double oxide with a unique multi-layered structure for low temperature NH_3-SCR. The optimal catalyst of Mn(0.25)/LDO showed efficient SCR activity in a temperature range of 150–300 °C with good resistance to both H_2O and SO_2. The promotional relationship between structure and performance in effects of Mn addition on surface of properties were investigated by the characterizations of SEM, TEM, XRD, FT-IR, BET, H_2-TPR, NH_3-TPD, XPS and DFT. Furthermore, the reaction mechanism of Mn(0.25)/LDO were proposed was revealed by *in situ* DRIFTS.

2. Experimental section

2.1. Catalyst preparation

Preparation of Co-Al layered double oxide supported MnO_x: For a typical synthesis process, 0.016 mol $Co(NO_3)_2 \cdot 6H_2O$, 0.008 mol $Al(NO_3)_3 \cdot 9H_2O$ and 0.100 mol urea were dissolved in 100 ml deionized water with vigorous stirring for 10 min. The resulting transparent solution was heated at 90 °C for 9 h in oven. When cooling to room temperature, the precipitate was collected by centrifugation, washed for 2–3 times with distilled water, and subjected to a freeze-drying process to obtain the Co-Al LDH precursors. Next, the required amount of Co-Al LDH and 50 wt % $Mn(NO_3)_2$ aqueous solution were added into a beaker containing distilled water, and stirred for 30 min to uniformly disperse the precursors. The 25% ammonia solution was dropped to the suspension until the pH rose to 9–10, the mixture was stirred for another 1 h at 25 °C. The target products were obtained by filtration, washed to neutrality with distilled water, dried at 60 °C for 8 h, and then calcined at 500 °C for 4 h in atmospheric air. A series of catalysts were denoted as Mn(x)/LDO, where x refers to the mass ratio of manganese to Co-Al LDH, the mass ratio in this work were 0.05, 0.1, 0.25 and 0.5, respectively. Meanwhile, MnO_x were manufactured by exactly the same method without the addition of Co-Al LDH, and the Co-Al LDO was resulted from the incineration of Co-Al LDH as a control. (The related preparation steps of Mn(x)/LDO were illustrated in Fig. 1, Mn(x)/LDH means uncalcined Mn(x)/LDO.)

2.2. Catalysts characterization

The powder XRD was performed to analyze crystal structure of catalysts on an X-ray diffractometer (Rigaku D/MAX 2500v/PC, λ = 0.15418 nm). The morphology and structure analyses were obtained by scanning electron microscopy (SEM, JEOL JEM-200CX), transmission electron microscopy (TEM, JEOL JEM-2100 F) and high-resolution TEM (HRTEM, JEOL JEM-2100 F), and the component of sample was characterized by energy-dispersive X-ray (EDX) analysis and elemental mapping. The XPS experiments were carried out on a surface analysis system (Thermal ESCALAB 250 spectrometer) equipped with Al Ka monochromatized radiation. The chemisorption analyzer was employed to measure the surface properties (BET specific surface area and pore size) of samples. The H_2 temperature-programmed reduction (H_2-TPR) and temperature-programmed desorption of NH_3 (NH_3-TPD) were carried out on a Micromerities Autochem 2920 instrument to measure the redox ability and NH_3 absorption ability of catalysts. Furthermore, the *in situ* Diffuse Reflectance Infrared Fourier Transform spectra (*in situ* DRIFTS) were collected on a Bruker Tensor 27 spectrometer to detect the adsorption behaviors and reaction pathway of reaction gas existing on the surface of Mn(0.25)/LDO. Prior to each experiment, the samples were exposed to the atmosphere of the nitrogen for 1 h at 350 °C. After the collection of background spectra was carried out from 100 to 350 °C, 500 ppm NH_3/N_2 or 500 ppm NO + 5% O_2/N_2 was introduced into the system, and then the *in situ* DRIFT spectra about samples' adsorption behaviors were taken with the ramping temperature (100–350 °C). For the exploration of the reaction path, the samples first completed the pre-adsorption of NO + O_2 or NH_3 at 150 °C, then 500 ppm NH_3/N_2 or 500 ppm NO + 5% O_2/N_2 was pumped into the system, the responded signal was recorded as a function of time.

In this work, electronic structure calculations based on DFT were conducted using the Vienna ab-initio simulation package (VASP) code, using the Perdew–Burke–Ernzerhof (PBE) functional within the generalized gradient approximation plus Hubbard model (GGA + U), while the value of U was set to 4.5 eV for Mn 3d states and 3.8 eV for Co 3d states [22–25]. For all the calculations, the plane-wave basis set with an energy cut off of 450 eV, the convergence energy and force were set at 10^{-5} eV and 0.01 eV/Å. In the calculation of Mn/LDO and Co-Al LDO, we choose Co_2AlO_4 as a simplified model of Co-Al LDO, using two Mn atoms substitute two Co atoms in the slab, which is in good agreement with the structural characteristics. Supercell models containing 169 atoms were constructed with periodically ($2 \times 2 \times 1$) for each model in optimization and ran to demonstrate the distribution of electron charge density for Mn loading on Co-Al LDO. During the optimization, all the atoms were relaxed without any constraint. The spin-polarized calculations were performed and a Monkhorst-pack grid $3 \times 3 \times 1$ k-point mesh was used.
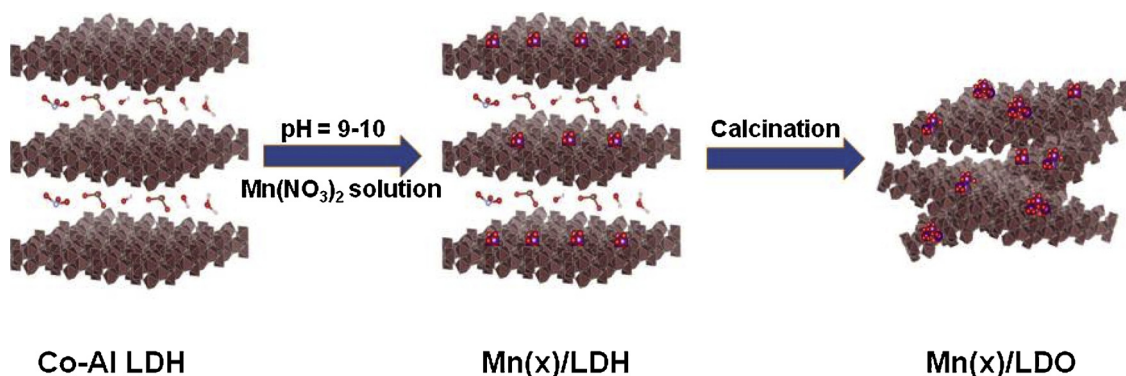

Fig. 1. Schematic illustration of the synthesis process.

2.3. Catalytic activity tests

The NH_3-SCR performance of samples were measured in a fixed-bed quartz reactor with a 10 mm inner diameter. The tested temperature was from 100 °C to 350 °C. The feed gas contained 500 ppm NO, 500 ppm NH_3, 5 vol % O_2, N_2 as a balance gas, 10 vol % H_2O (when needed), and 100 ppm SO_2 (when used). The total flow rate of inlet gases was 200 mL/min, and the gas hourly space velocity (GHSV) was about 40,000 h^{-1}. Prior to each test, 0.2 g 40–60 mesh sample was used. The component and concentration of outlet gas can be obtained by KM-940 flue gas analyzer (Kane International Limited, UK). The NO_x conversion rate and N_2 selectivity were evalued by the following equations:

$$NO_x \text{ conversion } (\%) = 100\% \times \frac{[NO_x]_{in} - [NO_x]_{out}}{[NO_x]_{in}}$$

$$N_2 \text{ selectivity } (\%) = 100\% \times (1 - \frac{2[N_2O]_{out} + [NO_2]_{out}}{[NH_3]_{in} + [NO_x]_{in} - [NH_3]_{out} - [NO_x]_{out}})$$

The $[NO_x]_{in}$ and $[NO_x]_{out}$ noted the inlet and outlet concentration at steady-state, separately ($[NO_x] = [NO] + [NO_2]$).

3. Results and discussion

3.1. Catalytic activity and resistance tests for NH_3-SCR

Fig. 2a shows the NO_x conversion as a function of temperature (100 to 350 °C) over Mn(x)/LDO catalysts with different mass ratios. Compared with pristine catalysts of Co-Al LDO and MnO_x, the different Mn(x)/LDO catalysts exhibited much better catalytic activities in the whole temperature. Especially for Mn(0.25)/LDO, the NO_x conversion achieved 73.9% at 100 °C and more than 95% from 150 to 300 °C. Additionally, the NO_x conversion of the Mn(0.25)/LDO could keep almost 100% in a GHSV range from 40,000 to 90,000 h^{-1} at 200 °C in Fig. 2b, but the catalytic activity of MnO_x then decreased with the increasing space velocity. These results show that MnO_x supported on Co-Al LDO can greatly promote the performance of the catalysts in the low temperature range. More than that, superior catalytic performance of Mn(x)/LDO imply that strong interaction and synergistic effect exist between MnO_x and Co-Al LDO species for NH_3-SCR reaction. The Mn(0.25)/LDO was thus chosen for further study. Various characterizations were carried out to investigate the relationship between structure and catalytic activities.

The presence of vapor and sulfur dioxide in the combustion exhaust were known as two key deactivation causes of SCR catalysts. Therefore, the resistance tests to H_2O and SO_2 of Mn(0.25)/LDO and MnO_x were performed with feed gas containing the additional 10 vol. % H_2O or 100 ppm SO_2 at 200 °C for 24 h under a GHSV of 40,000 h^{-1}. The relevant results were shown in the Fig. 3(a–c). As shown in Fig. 3a, the

NO conversion of Mn(0.25)/LDO and MnO_x decreased from 100% and 94.8% to 98.1% and 50.7% after 10 vol. % H_2O vapor was injected into the feed gas atmosphere. After that, cutting off the H_2O vapor immediately brought the NO_x conversion back to original level, respectively, suggesting that Mn(0.25)/LDO possesses a better H_2O vapor tolerance and deactivation of H_2O vapor is reversible. Meanwhile, the hydrothermal aging treatment of Mn(0.25)/LDO was carried out in Fig. S2, the results show that Mn(0.25)/LDO has a good hydrothermal aging resistance. In addition, the effects of SO_2 over Mn(0.25)/LDO and MnO_x are exhibited in Fig. 3b. The NO_x conversion dropped from 100% and 94.8% to 93.2% and 81.3% with the introduction of 100 ppm SO_2, indicating Mn(0.25)/LDO exhibited more splendid tolerance of sulfur dioxide than MnO_x. A similar tendency exists in the two catalysts that the activity of samples revealed a decreasing tend at initial few hours and then maintained a stable state, but the NO_x conversion could not recovery to the original state after switching off the SO_2. The combined impact of water vapor and sulfur dioxide was also studied in details (Fig. 3c). The NO_x conversion of Mn(0.25)/LDO decreased from 100% to 76.5% after the co-existence of 10 vol.% H_2O and 100 ppm SO_2. However, NO_x conversion of MnO_x was decreased from 94.8% to 41.1%. Therefore, it is showed that the Mn(0.25)/LDO obtain well SO_2/H_2O durability. Nevertheless, when the H_2O and SO_2 was removed, the catalytic performance of Mn(0.25)/LDO recovered to 92%. The deNO$_x$ activity of catalysts were not completely regenerated, suggesting that the irreversible deactivation existed in the Mn(0.25)/LDO and MnO_x. According to the previous works, two main factors can be matched with the deactivation of the samples. On one hand, ammonium sulfate species can form on the surface of catalyst and block the active sites, causing the reversible deactivation. On the other hand, stable sulfate species generated during the sulfation process, such as manganese sulfate, leading to an irreversible deactivation [26]. Fig. 3d showed the thermal stability tests of the catalysts at 200 °C, and the NO_x conversion of Mn(0.25)/LDO and MnO_x maintained stability at 100%, 94.8% during 50 h, respectively. Besides, The N_2 selectivity (Fig. S1) of Co-Al LDO, Mn(0.25)/LDO and MnO_x were also analyzed in the range of 50 °C to 350 °C, and Mn(0.25)/LDO performed better than Co-Al LDO and MnO_x. Through the above experimental results, we have concluded that MnO_x supported on Co-Al layered double oxide has high stability and strong resistance to H_2O and SO_2.

3.2. Microstructure and micromorphology analysis

In order to explore the relationship between the structural with performance in details, we performed microstructure and micromorphology analysis. To obtain structural information of the Co-Al LDO, Mn(x)/LDO and MnO_x catalysts, XRD patterns were depicted in Fig. 4. The Co-Al LDO mainly exhibited Co_3O_4 spinel phase (PDF#42-1467) [27]. The strongest diffraction peak located at 36.8° is ascribed to
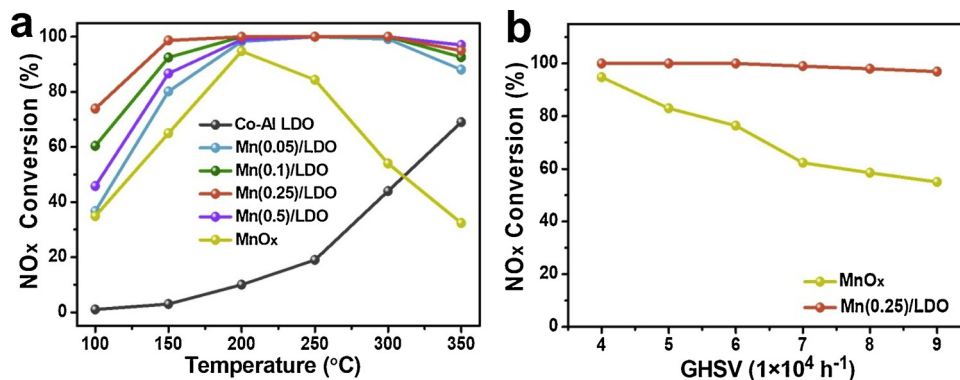

Fig. 2. (a) NO_x conversion of MnO_x, Mn(x)/LDO and Co-Al LDO. Reaction conditions: [NO] = [NH_3] = 500 ppm, [O_2] = 5 vol.%, GHSV = 40,000 h^{-1} and N_2 as balance. (b) NO_x conversion of MnO_x and Mn(0.25)/LDO under different GHSV, reaction temperature at 200 °C.

Fig. 3. Resistance tests of MnO_x and Mn(0.25)/LDO. (a) H_2O resistance, (b) SO_2 resistance, (c) $H_2O + SO_2$ resistance, (d) thermal stability test. Reaction conditions: $[NH_3] = [NO] = 500$ ppm, $[O_2] = 5$ vol.%, $[SO_2] = 100$ ppm (when used), $[H_2O] = 10$ vol.% (when used), N_2 balance and GHSV = 40,000 h^{-1}, reaction temperature at 200 °C.
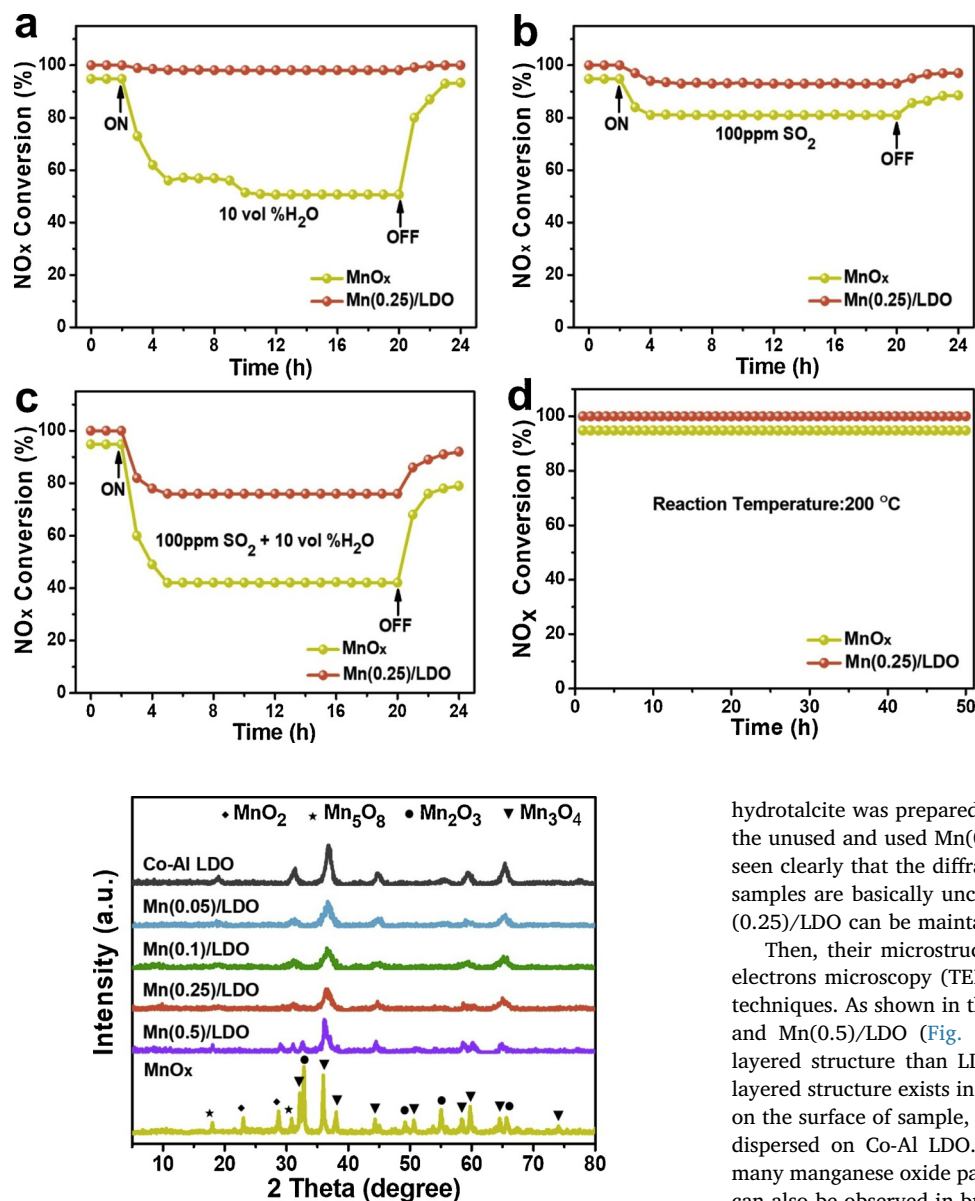

Fig. 4. The Powder XRD patterns of Co-Al LDO, Mn(x)/LDO and MnO_x.

the (311) reflection in Co_3O_4. In addition, the reflection peaks at 18.9°, 31.2°, 45°, 59.4° and 65.3°, corresponding to the (111), (220), (400), (511) and (440) planes of Co_3O_4 spinel phase, respectively. For Mn(x)/LDO samples, after the addition of manganese element, there is no obvious diffraction peak of manganese oxide species (when x is 0.05-0.25). Meanwhile, with the adding of manganese species, the peak intensity of Co-Al LDO got lower, which was due to manganese species could reduce the crystallization of Co-Al LDO and thus enhance the dispersion of manganese oxide species on the surface. It has been reported that the decrease of crystallization degree will lead to the increase of surface adsorbed oxygen, thus promoting the activity of SCR. [28]. Whereas, some reflection diffraction peaks at 18.0°, 28.9°, 32.3°, 36.1°, 58.5° and 59.8° of Mn(0.5)/LDO, corresponding to the (101), (112), (103), (211), (321) and (224) planes of Mn_3O_4 (PDF# 24-0734) [29]. What's more, the diffraction peaks attributed to Al_2O_3 could not be found from the XRD patterns in all catalysts, indicating that amorphous Al_2O_3 matrix may act as a carrier to stabilize and disperse active sites [30]. Meanwhile, in our work, LDH was the most important precursor for the synthesis of LDO. As shown in Figs. S3 and S4, the XRD pattern and the FT-IR spectra of Co-Al LDH demonstrated that Co-Al

hydrotalcite was prepared successfully. Moreover, the XRD patterns of the unused and used Mn(0.25)/LDO are displayed in Fig. S5. It can be seen clearly that the diffraction peak position and intensity of the two samples are basically unchanged, indicating the microstructure of Mn(0.25)/LDO can be maintained during the reaction process.

Then, their microstructure was further studied using transmission electrons microscopy (TEM) and scanning electron microscopy (SEM) techniques. As shown in the SEM images of Co-Al LDO, Mn(0.25)/LDO and Mn(0.5)/LDO (Fig. 5a–c), Co-Al LDO possesses a more multi-layered structure than LDH (Fig. S6a), evidently. The similar multi-layered structure exists in Mn(0.25)/LDO and there is no MnO_x species on the surface of sample, indicating that manganese species are highly dispersed on Co-Al LDO. However, for the Mn(0.5)/LDO, there are many manganese oxide particles on the surface of Mn(0.5)/LDO, which can also be observed in bulk MnO_x (Fig. S6b). The same results can be obtained from the typical HRTEM images. As expected, in the Co-Al LDO, the lattice spacing of 0.202 nm and 0.286 nm are corresponded to the planes of (400) and (220) in the Co_3O_4 [31] (Fig. 5d, Fig. S7a). For the Mn(0.25)/LDO, the lattice fringe (0.204 nm) is assigned to the (400) plane of Co_3O_4. Additionally, there is another spacing distance (0.250 nm) in the Fig. 5e and Fig. S7b, which can be attributed to the plane of (311) in the Co_3O_4 [32]. It is observed that (400) plane of Co_3O_4, a slight increase (0.002 nm) of interplanar spacing is detected with manganese loading from the Fig. 5d–e, which is ascribed to the doping Mn species into Co-Al LDO occurs at the interface and this may lead structural deformation in Co_3O_4 lattice and promote the interaction between manganese and supports [33,34]. The obtained results are in good agreement with those of XRD analysis. Nevertheless, we observed two different phases exist in the Mn(0.5)/LDO (Fig. 5f, S7c). The spacing distances are separately 0.481 nm and 0.248 nm, which belonged to the (111) plane of Co_3O_4 and the plane of (211) in Mn_3O_4 (PDF# 24-0734) [35–37]. That suggested manganese oxide species are formed on the surface of Mn(0.5)/LDO, which can also be obtained from XRD. Furthermore, the TEM-EDX mapping (Fig. 5g–k, S7d) are further confirmed that Co, Mn, Al and O were uniformly distributed over the Mn(0.25)/LDO, implying that manganese species were highly dispersed on the Co-Al LDO.
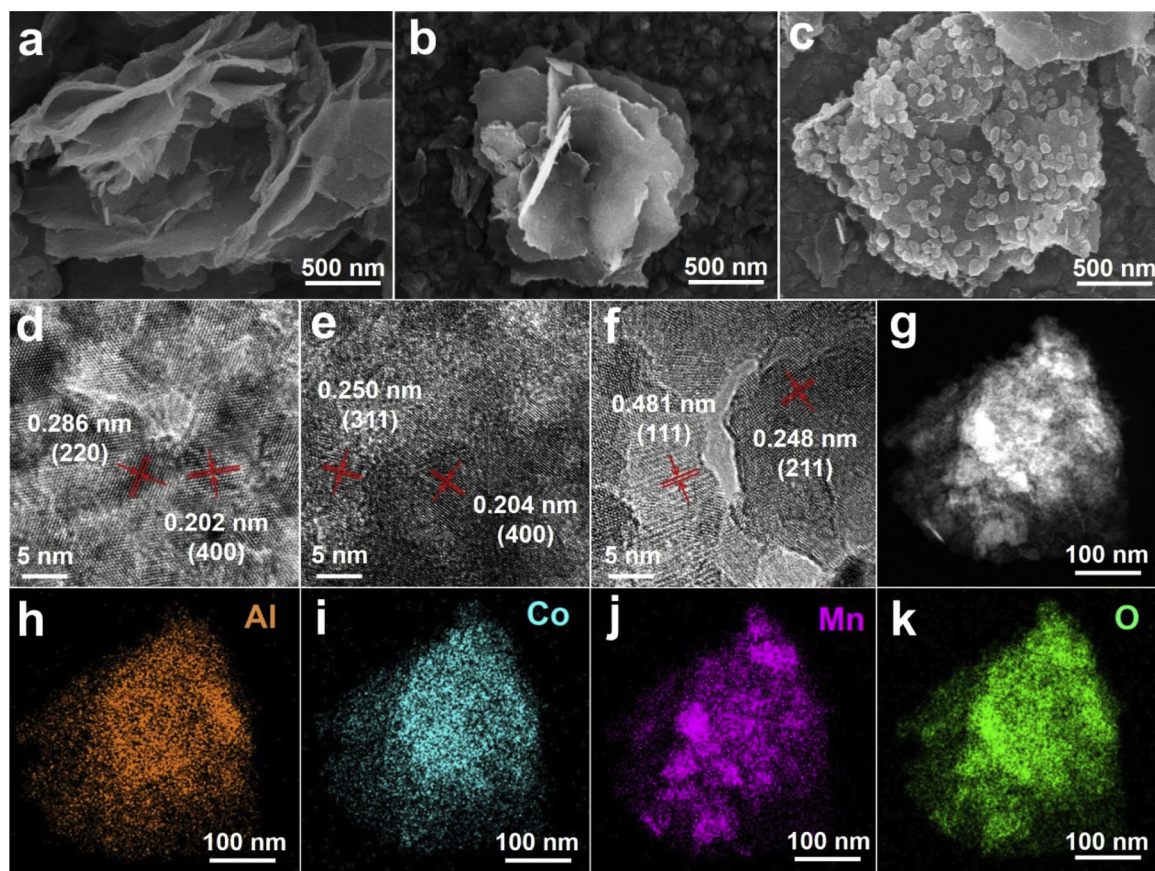
Fig. 5. SEM and HRTEM images of Co-Al LDO (a, d), Mn(0.25)/LDO (b, e), Mn(0.5)/LDO (c, f) and EDX mapping of the Mn(0.25)/LDO (g–k).

3.3. The surface property analysis of catalyst

To explore the change of specific surface area and pore structure after the addition of manganese element, the N$_2$ adsorption-desorption isotherms of the Co-Al LDO, MnO$_x$ and Mn(x)/LDO catalysts were performed (Fig. 6a). Moreover, the results of specific surface area, pore volume and pore size distribution are also listed in Table 1. The adsorption-desorption isotherms of all the Mn(x)/LDO catalysts are in accordance with the type IV isotherms with type H1 hysteresis loops [38], which is corresponding to the mesoporous structure. This result can also be confirmed from the pore size distribution, which is basically concentrated around 3 to 4.5 nm (Fig. 6b). There is an interesting phenomenon that Mn(0.05)/LDO showed the greater specific surface area than Co-Al LDO. According to previous literature reports, this may be caused by the intercalation of a low content Mn ions into the support

Table 1
Summary of textual parameters of the samples.

Samples	Specific area (m^2/g)	Pore volume (cm^3/g)	Average pore diameter (nm)
Co-Al LDO	152.50	0.32	3.40
Mn(0.05)/LDO	183.38	0.33	3.42
Mn(0.1)/LDO	179.46	0.32	3.43
Mn(0.25)/LDO	155.10	0.31	3.48
Mn(0.5)/LDO	117.75	0.30	3.51
MnO$_x$	14.24	0.08	—

at the interface [39]. Liang et al reported that the isomorphic substitution was one of the ways to remove heavy metal ions in hydrotalcite materials [40]. Another investigation also illustrated that the shift of Bragg angles in (Mg, Mn)$_2$Al LDH–Cl was due to the
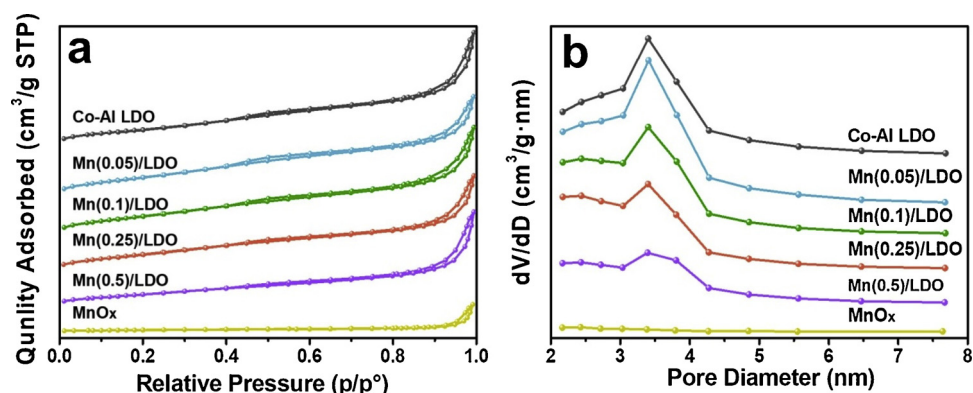

Fig. 6. (a) Nitrogen adsorption–desorption isotherm, (b) Pore size distribution of Co-Al LDO, Mn(x)/LDO and MnO$_x$.

replacement between the bigger size Mn^{2+} and Mg^{2+} [20]. Considering these points, the analogous cation exchange processes can be allowed between the Mn^{2+} and Co-Al LDH. Therefore, we can deduce that the lattice distortion can be assigned to the supersession of the larger size Mn^{2+} to Co^{2+}, resulting in the greater specific surface area in the Mn (0.05)/LDO. Besides, there is a downtrend of the surface area from Mn (0.05)/LDO to Mn(0.5)/LDO, which is related to the bonding of Mn^{2+} and the surface hydroxyl groups of Co-Al LDH [21]. The declining phenomenon became more and more significant with the rising quantity of manganese species, which also can be observed the formation of manganese oxide bulks in the SEM of Mn(0.5)/LDO. As a result, a reasonable inference can be made that Mn(x)/LDO was undergoing such a process that manganese ions embedded the support lattice with a low content, and starting monolayer or multi-layer dispersion until the appearance of manganese oxide bulks with the higher manganese loading. Compared with Co-Al LDO, it is noteworthy that the specific surface area of Mn(x)/LDO increases except the Mn(0.5)/LDO. This is resulted from the more manganese ions dispersion on the surface of Mn (0.5)/LDO. On the whole, the increasing of specific surface area of Mn (x)/LDO series catalysts by the addition of Mn could provide abundant adsorption sites of reactant molecules, contributing to the higher catalytic activity.

3.4. Redox properties and surface acidity

The redox property is an important index to evaluate the performance of catalysts, and H_2-TPR technology provides an effective way in measuring the reducibility of the Mn(x)/LDO catalysts. As shown in Fig. 7a, the H_2 consumption of 200–300 °C is related to the reduction of Co^{3+}-Co, 300–500 °C is attributed to the reduction of Co^{2+}-Co^0, Mn^{4+}-Mn^{3+}, Mn^{3+}-Mn^{2+}, and the reduction peak at 500–800 °C can be assigned to the reduction of CoO and cobalt aluminate [17]. It can be seen clearly that the reduction peak at 500–800 °C shifts to a higher temperature (from 535 °C to 623 °C) with the increase of Mn content. This result reveals that there is the interaction between manganese species and carriers. Meanwhile, Mn(0.5)/LDO displays a small protuberant peak at around 438 °C, which can be assigned to the reduction procession of Mn_2O_3-Mn_3O_4 [39]. This brings to light that manganese oxide bulks emerge in Mn(0.5)/LDO, which keeps in line with previous XRD and SEM results. For the pristine MnO_x, the peaks located at 305 °C and 412 °C are related to the reduction of MnO_2-Mn_2O_3 and Mn_2O_3-Mn_3O_4, respectively. A marked shift toward lower temperature is acquired for Mn(x)/LDO series catalysts with Mn addition, which accounts for the outstanding low temperature catalytic performance.

The surface acidic site is closely related to NH_3 adsorption behavior, which plays a vital role in the NH_3-SCR reaction. As depicted in Fig. 7b, the profiles of the Mn(x)/LDO samples present a broad desorption peak from 100 °C to 400 °C. It is a powerful evidence that manganese addition could significantly increase the positive charge density around Mn would lead to an increased number of Lewis acid sites. Meanwhile, we

found that the change of the intensity perfectly synchronizes with the SCR activity of Mn(x)/LDO catalysts. On the basis of the previous works, the NH_3 adsorption of 100–200 °C can be attributed to absorption of the NH_4^+ ion associated with the Brønsted acid sites, and the peaks above 200 °C are assigned to NH_3 coordination of the Lewis acid sites. Moreover, the stability of Lewis acid site is better than Brønsted acid site, and Lewis acid site play works in a wider temperature [41]. It can be clearly observed that the NH_3 desorption peak of Mn(x)/LDO shifts to low temperatures significantly in Fig. 7b, which contributed to the excellent low-temperature SCR activity of Mn(x)/LDO. In addition, when it comes to the peak area of NH_3 desorption, Mn(0.25)/LDO is the largest, followed by Co-Al LDO, Mn(0.1)/LDO, Mn(0.5)/LDO and Mn (0.05)/LDO respectively. The variation of NH_3 desorption peak area of Mn(x)/LDO is in perfect agreement with the corresponding the $deNO_x$ performance. In the NH_3-TPD profile of Mn(0.25)/LDO, the ammonia adsorption appears on the whole temperatures, and a stronger signal occurs above 200 °C, indicating that more Lewis acid sites exist in the sample. These features of Mn(0.25)/LDO contribute to the remarkable low temperature activity.

3.5. Chemical composition and electronic States

The XPS measurement is employed to elaborate the valence of diverse elements on the sample surface (Fig. 8). The Mn2p, O 1 s, Co2p and Al spectra are displayed in Fig. 8a–c and Fig. S8, and the oxidation state ratios of elements are summarized in Table 2. Take the standardized C1 s as a reference (284.6 eV), the binding energy is calibrated in all catalysts. As shown in Fig. 8a, the two protuberant peaks corresponding to Mn $2p_{3/2}$ and Mn $2p_{1/2}$ can be seen. After the peak-fitting deconvolution is performed, the Mn $2p_{3/2}$ peak can be divided into four peaks, corresponding to Mn^{2+} (640.7–641.1 eV) Mn^{3+} (641.6–642.2 eV) Mn^{4+} (643.0–643.6 eV) and the satellite peak (644.5–645.2 eV) [42–44]. It is a significant fact that the binding energy position of Mn $2p_{3/2}$ moves to the higher value after the introduction of manganese. It can be demonstrated that the chemical environment of manganese in Mn(x)/LDO is different from MnO_x, suggesting that there is an interaction between manganese species and supports. As reported, Mn^{4+} usually plays an irreplaceable role in SCR reaction. The redox cycle of Mn^{4+} species favors the SCR activity at low temperatures, which can be attributed to the promotion of oxidation from NO to NO_2 [44,45]. As a result, the more Mn^{4+} exist, the better catalytic activity the samples get. As listed in the Table 2, the Mn (0.25)/LDO is the summit in all Mn^{4+}/Mn values and the relative ratio of Mn^{4+}/ Mn^{3+}, which determines the outstanding SCR performance.

For the spectra of Co 2p, there are two distinct peaks, and the peak of Co $2p_{3/2}$ is fitted into three peaks in Fig. 8b. The peak centered in 780.3–780.5 eV could be ascribed to Co^{3+}, the peak located at 781.8–782.2 eV is assigned to Co^{2+}, and another peak of 786.5–787 eV is corresponded to the satellite of cobalt. [46]. According to previous report, the Co^{3+} species play an critical role in NH_3 chemisorption
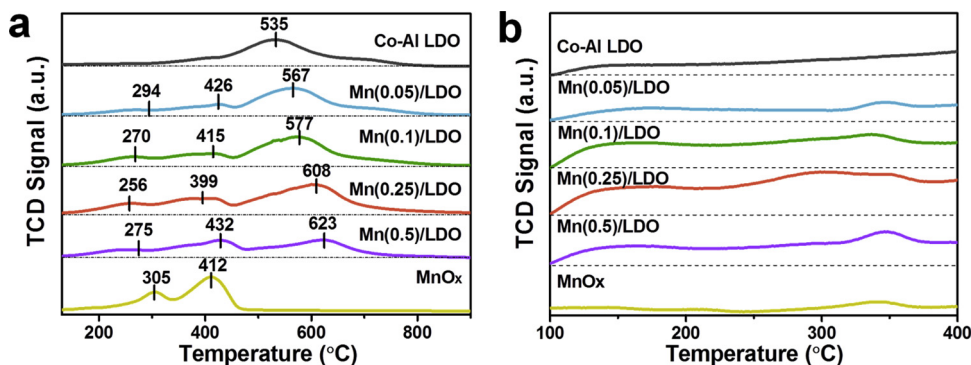

Fig. 7. (a) H_2-TPR and (b) NH_3-TPD profiles of Co-Al LDO, Mn(x)/LDO and MnO_x.
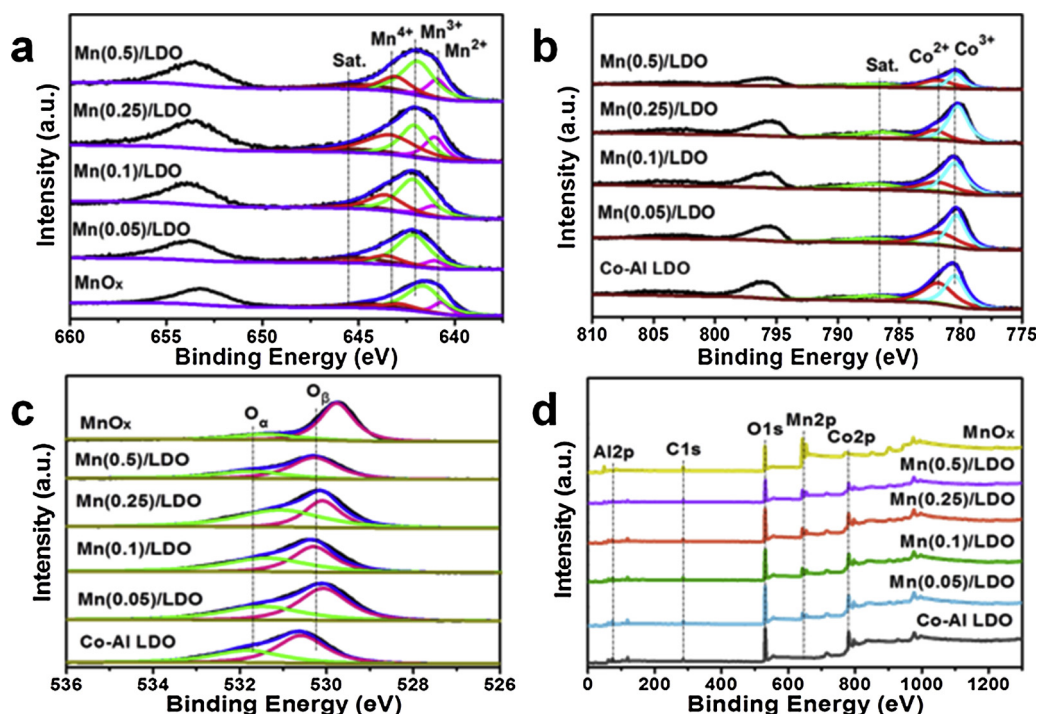
Fig. 8. XPS spectra for Co-Al LDO, Mn(x)/LDO, MnOx (a) Mn 2p (b) Co 2p (c) O 1s (d) wide-scan spectra.

[35]. In general, It is recognized that the more Co^{3+} is desirable for redox performance over the surface of catalysts, which can result in more preferable catalytic activity [47]. The Table 2 lists the relative surface content of Co^{3+} (Co^{3+}/Co). Among all samples, Mn(0.25)/LDO owns more abundant Co^{3+}, which is in good agreement with the obvious enhancement of catalytic activity.

Two main signals of oxygen species were defined by performing the peak-fitting deconvolution in Fig. 8c. Based on literatures, the peak located at 529.7–530.6 eV can be assigned to the lattice oxygen species (O_β), and surface-adsorbed oxygen species (O_α) is corresponded to the peak of 531.1–531.8 eV. It is well known that O_α is more active than O_β, the higher mobility of the O_α supported the better performance in oxidation reaction [48]. As presented in the Table 2, the ratio of the $O_\alpha/(O_\alpha + O_\beta)$ increased gradually (when x is from 0.05 to 0.25). This can be owing to the induction of the charge imbalance, unsaturated chemical bonds and vacancies on the surface of Mn(x)/LDO due to the co-operation and cation exchange between manganese and carriers. By contrast, a obvious decrease occurred in Mn(0.5)/LDO with formation of manganese oxide bulks. In addition, the Al spectra of Co-Al LDO and Mn(x)/LDO (Fig. S8) show displacements as well, indicating the interaction between manganese and the Co-Al LDO.

In order to further confirm the electronic inductive effect between Mn and Co-Al LDO, we also constructed the electron density difference based on DFT results (Fig. 9) and found the manganese addition could significantly increase a number of Lewis acid sites. The electron
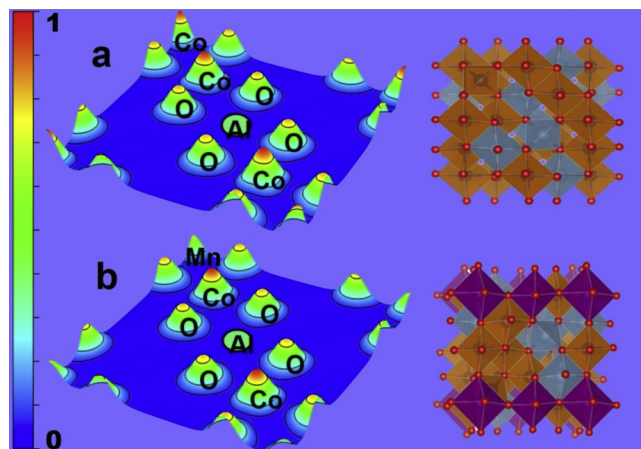

Fig. 9. The electron density difference and atom model of (a) Co-Al LDO and (b) Mn(x)/LDO (Electron accumulation and depletion are marked by red and blue areas, respectively). (For interpretation of the references to colour in this figure legend, the reader is referred to the web version of this article).

transfers from Mn to the coordinated oxygen and further to the neighboring Co and Al atoms can be clearly observed. Therefore, more charge accumulation around Mn can be obtained in Co-Al LDO, which is in good accordance with the NH$_3$-TPD and *in situ* DRIFTS results in

Table 2
The Valence Ratios of Surface Elements.

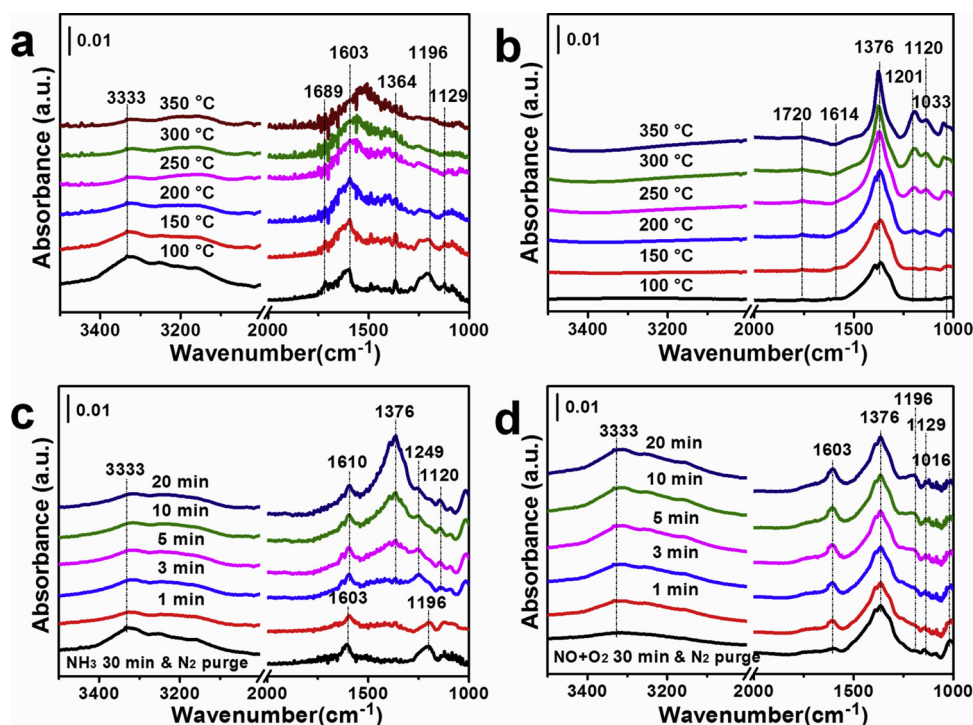| Catalysts	Mn 2p		Co 2p		O 1s	
	Mn^{4+}/Mn	Mn^{4+}/Mn^{3+}	Co^{3+}/Co	Co^{3+}/Co^{2+}	$O_\alpha/(O_\alpha + O_\beta)$	O_α/O_β
Co-Al LDO	—	—	0.41	0.99	0.38	0.62
Mn(0.05)/LDO	0.15	0.26	0.46	1.26	0.41	0.69
Mn(0.1)/LDO	0.27	0.50	0.5	1.91	0.51	1.06
Mn(0.25)/LDO	0.39	1.13	0.57	3.18	0.60	1.50
Mn(0. 5)/LDO	0.20	0.41	0.37	0.98	0.32	0.47
MnO$_x$	0.12	0.20	—	—	0.20	0.26

Fig. 10. *in situ* DRIFTS spectra of (a) NH_3 adsorption, (b) NO adsorption over Mn(0.25)/LDO in the temperature range of 100–350 °C; *in situ* DRIFT spectra of transient reactions at 150 °C over Mn(0.25)/LDO catalyst between (c) preadsorbed NH_3 and NO + O_2, (d) preadsorbed NO + O_2 and NH_3 as a function of time.

this section. It is worth noting that the increment in positive charge density around Mn atoms along with imbalance of the charge density distribution would lead to an increased number of Lewis acid sites, which can be beneficial to the adsorption of NO and NH_3 [49].

3.6. Reaction mechanism over the Mn(0.25)/LDO catalyst

To investigate the NH_3-SCR reaction mechanism of Mn(x)/LDO, the *in situ* DRIFTS were performed to explore the adsorption behaviors of the reactant molecules and monitor the crucial intermediates. Considering that NH_3 adsorption and activation is the initial and critical step of the SCR process [50]. The typical *in situ* DRIFTS spectra of NH_3 adsorption over Mn(0.25)/LDO sample were taken with the ramping temperature (Fig. 10a). The band at 3333 cm^{-1} can be assigned to the N−H stretching vibration of the associated NH_3, and the bands located at 1603, 1196 and 1129 cm^{-1} are ascribed to the NH_3 coordinated to the Lewis acid sites [51,52] were clearly observed. Besides, the shoulder at 1689 cm^{-1} and 1364 cm^{-1} are attributed to the asymmetric and symmetric bending vibrations (ν_{as} and ν_s) of the NH_4^+ on Brønsted acid sites, which is in consistent with the analysis of NH_3-TPD. What's more, it can be clearly observed that the signal of the bands at 1196, 1129 and 3333 cm^{-1} evidently decreased with ramping temperature. However, the intensity of 1603 cm^{-1} displayed a slight drop even at high temperature, indicating that there is still a considerable amount of adsorbed ammonia on the catalyst surface, which contribute to the wide working temperature window and manifesting that Lewis acid sites play a main role in the SCR reaction.

The *in situ* DRIFTS of NO + O_2 adsorption capacity over the Mn (0.25)/LDO sample at different temperatures were also carried out (Fig. 10b). The distinct bands assigned to monodentate nitrate (1033 cm^{-1}), ν_{as} and ν_s modes of monodentate nitrite (1120, 1201 cm^{-1}) and ionic nitrate(1376 cm^{-1}), respectively [28,52,53]. In addition, the bands at 1614 cm^{-1} and 1720 cm^{-1} can be separately assigned to the asymmetric frequency of gaseous NO_2 and trans-$(NO)_2$. Furthermore, it's obvious that the peaks of monodentate nitrate and monodentate nitrite appear with the increasing temperature, which has

been proved that is an important active species over Manganese based catalyst in SCR reaction [54,55].

The transient reactions over Mn(0.25)/LDO in a flow of NO + O_2 / NH_3 after the sample was pre-adsorbed NH_3 / NO + O_2 at 150 °C were further explored by *in situ* DRIFTS spectra (Fig. 10c–d). Prior to the reaction between NO + O_2 and pre-adsorbed NH_3 (Fig. 10c). After the introduction of NO + O_2, the adsorbed NH_3 species (1603 and 1196 cm^{-1}) bound to Lewis acid sites show a significant decrease after 1 min and disappear in the 3 min, indicating that the coordinated NH_3 species can quickly participate in the SCR reaction. Meanwhile, new bands ascribed to the gaseous NO_2 (1610 cm^{-1}), ionic nitrate (1376 cm^{-1}) and monodentate nitrite (1120 cm^{-1}, 1249 cm^{-1}) appear and enhance as time goes on, indicating that nitrogen oxides start to absorb on the surface of catalyst [28]. The reaction between NO + O_2 and pre-adsorbed NH_3 reveal that the proposed Eley-Rideal mechanism exists in the SCR reaction process [14]. In contrast, *in situ* DRIFTS of reactions between NH_3 and pre-adsorbed NO + O_2 species was also collected (Fig. 10d). After the introduction of NH_3, there was no obvious change about the ionic nitrate species (1376 cm^{-1}). Monodentate nitrate (1016 cm^{-1}) showed rapid decrease in intensity, manifesting that this nitrate species was reactive in the SCR reaction. Moreover, the intensity of 1129 cm^{-1}, 1196 cm^{-1} and 1603 cm^{-1} (attributed to coordinated NH_3) gradually appears and increases due to the introduction of NH_3 from 1 min to 20 min. In addition, the reaction of NH_3 with pre-adsorbed NO + O_2 is more difficult than the reverse condition.

From the *in situ* DRIFTS spectra analysis we can conclude that the NH_3-SCR over Mn(0.25)/LDO mainly follows E-R mechanism between absorbed NH_3 species with the gaseous NO at low temperature [56]. Concerning the reaction pathway on the Mn(x)/LDO, we give a following detailed explanation (Fig. 11). Obviously, when the flow of ammonia passed by the surface of catalyst, NH_3 is immediately adsorbed to the Lewis acid centers and accompanying with the formation of coordinated NH_3 and NH_2 intermediates [57], then the associated NH_3 and NH_2 intermediates can directly react with the gaseous NO to form the N_2 and H_2O. Secondly, the NH_4NO_2 and NH_4NO_3 formation by the combination between the adsorbed NH_3 species with NO_2^-
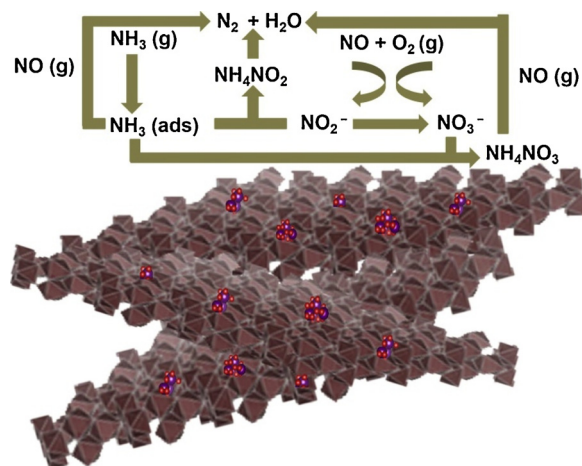
Fig. 11. The NH$_3$-SCR reaction mechanism on Mn(0.25)/LDO.

species, then the NH$_4$NO$_2$ decompose into the N$_2$ and H$_2$O [41]. Meanwhile, NH$_4$NO$_3$ can react with NO (g) follow the reaction process (NH$_4$NO$_3$ + NO → NO$_2$ + N$_2$ + 2H$_2$O). However, we can observe this reaction process is relatively slow and L-H mechanism plays a secondary role over the Mn(x)/LDO for low temperature NH$_3$-SCR.

4. Conclusions

In summary, a novel highly dispersed MnO$_x$ on Co-Al layered double oxide with a unique multi-layered structure for low temperature NH$_3$-SCR were successfully prepared by conventional impregnation. What's more, the Mn(0.25)/LDO exhibited superior a great H$_2$O and SO$_2$ tolerance, which has the potential of practical application. The introduction of manganese species decreased the crystallinity of Co-Al LDO, generating more crystal defects, which contributed to the increase of Mn^{4+} and chemisorbed oxygen species and improved the SCR activity. Meanwhile, Mn(x)/LDO series catalysts have relatively large BET surface area, providing more adsorption sites of reactant molecules, the H$_2$-TPR analysis suggested that Mn addition affected the redox ability of the samples. The NH$_3$-TPD, DFT and *in situ* DRIFTS of ammonia adsorption showed that the surface acidity of Mn(x)/LDO was enhanced by Mn addition, and Lewis acid sites acted as a key role in NH$_3$-SCR reaction. Furthermore, the proposed reaction mechanism of Mn(x)/LDO was revealed by *in situ* DRIFTS and the E-R mechanism mainly existed in the SCR reaction.

Declaration of Competing Interest

The authors declare that they have no known competing financial interests or personal relationships that could have appeared to influence the work reported in this paper.

Appendix A. Supplementary data

Supplementary material related to this article can be found, in the online version, at doi:https://doi.org/10.1016/j.apcatb.2019.117983.

References

[1] W. Yao, X. Wang, Y. Liu, Z. Wu, Appl. Surf. Sci. 467–468 (2019) 439–445.
[2] R. Wang, Z. Wang, X. Xiang, R. Zhang, X. Shi, X. Sun, Chem. Commun. 54 (2018) 10340–10342.
[3] X. Li, T. Li, Y. Ma, Q. Wei, W. Qiu, H. Guo, X. Shi, P. Zhang, A.M. Asiri, L. Chen, B. Tang, X. Sun, Adv. Energy. Mater 8 (2018) 1801357.
[4] Z. Wang, F. Gong, L. Zhang, R. Wang, L. Ji, Q. Liu, Y. Luo, H. Guo, Y. Li, P. Gao, X. Shi, B. Li, B. Tang, X. Sun, Adv. Sci. 6 (2019) 1801182.
[5] X. Zhang, T. Wu, H. Wang, R. Zhao, H. Chen, T. Wang, P. Wei, Y. Luo, Y. Zhang, X. Sun, ACS Catal. 9 (2019) 4609–4615.
[6] J. Li, H. Chang, L. Ma, J. Hao, R. Yang, Catal. Today 175 (2011) 147–156.
[7] P.G. Smirniotis, D.A. Peña, B.S. Uphade, Angew. Chem. Int. Ed. 40 (2001) 2479–2481.
[8] L. Han, M. Gao, C. Feng, L. Shi, D. Zhang, Environ. Sci. Technol. 53 (2019) 5946–5956.
[9] L. Han, M. Gao, J.Y. Hasegawa, S. Li, Y. Shen, H. Li, L. Shi, D. Zhang, Environ. Sci. Technol. 53 (2019) 6462–6473.
[10] L. Yan, Y. Gu, L. Han, P. Wang, H. Li, T. Yan, S. Kuboon, L. Shi, D. Zhang, ACS Appl. Mater. Interface 11 (2019) 11507–11517.
[11] K. Zha, L. Kang, C. Feng, L. Han, H. Li, T. Yan, P. Maitarad, L. Shi, D. Zhang, Environ. Sci.: Nano 5 (2018) 1408–1419.
[12] H. Hu, S. Cai, H. Li, L. Huang, L. Shi, D. Zhang, J. Phys. Chem. C 119 (2015) 22924–22933.
[13] L. Chen, F. Yuan, Z. Li, X. Niu, Y. Zhu, Chem. Eng. J. 354 (2018) 393–406.
[14] L. Kang, L. Han, J. He, H. Li, T. Yan, G. Chen, J. Zhang, L. Shi, D. Zhang, Environ. Sci. Technol. (2019) 938–945.
[15] H. Hu, S. Cai, H. Li, L. Huang, L. Shi, D. Zhang, ACS Catal. 5 (2015) 6069–6077.
[16] J. Zhang, Z. Li, Y. Chen, S. Gao, X.W.D. Lou, Angew. Chem. Int. Ed. 57 (2018) 10944–10948.
[17] X. Wu, Y. Feng, Y. Du, X. Liu, C. Zou, Z. Li, Appl. Surf. Sci. 467–468 (2019) 802–810.
[18] Q. Yan, S. Chen, C. Zhang, Q. Wang, B. Louis, Appl. Catal. B 238 (2018) 236–247.
[19] S. Chen, Q. Yan, C. Zhang, Q. Wang, Catal. Today 327 (2019) 81–89.
[20] M.C. Richardson, P.S. Braterman, J. Mater. Chem. 19 (2009) 7965.
[21] D. Zhao, G. Sheng, J. Hu, C. Chen, X. Wang, Chem. Eng. J. 171 (2011) 167–174.
[22] G. Kresse, J. Hafner, Phys. Rev. B 47 (1993) 558–561.
[23] G.K.J. Furthmiiller, Comp. Mater. Sci. 6 (1996) 15–50.
[24] D.M.C.B.J. Alder, Phys. Rev. Lett. 45 (1980) 566–569.
[25] H. Zheng, W. Song, Y. Zhou, S. Ma, J. Deng, Y. Li, J. Liu, Z. Zhao, J. Phys. Chem. C 121 (2017) 19859–19871.
[26] E. Park, M. Kim, H. Jung, S. Chin, J. Jurng, ACS Catal. 3 (2013) 1518–1525.
[27] S. Mo, S. Li, W. Li, J. Li, J. Chen, Y. Chen, J. Mater. Chem. A 4 (2016) 8113–8122.
[28] D. Meng, W. Zhan, Y. Guo, Y. Guo, L. Wang, G. Lu, ACS Catal. 5 (2015) 5973–5983.
[29] Y. Jian, M. Ma, C. Chen, C. Liu, Y. Yu, Z. Hao, C. He, Catal. Sci.Technol. 8 (2018) 3863–3875.
[30] S. Li, S. Mo, J. Li, H. Liu, Y. Chen, RSC Adv. 6 (2016) 56874–56884.
[31] Y. Lu, Y. Wang, Y. Zou, Z. Jiao, B. Zhao, Y. He, M. Wu, Electro. Chem. Commun. 12 (2010) 101–105.
[32] X. Lou, D. Deng, J.Y. Lee, J. Feng, L.A. Archer, Adv. Mater 20 (2008) 258–262.
[33] P. Wang, Z. Shen, Y. Xia, H. Wang, L. Zheng, W. Xi, S. Zhan, Adv. Funct. Mater. 29 (2019) 1807013.
[34] S. Shen, L. Zhao, Z. Zhou, L. Guo, J. Phys. Chem. C 112 (2008) 16148–16155.
[35] B. Meng, Z. Zhao, X. Wang, J. Liang, J. Qiu, Appl. Catal. B 129 (2013) 491–500.
[36] X. Wang, Y. Fan, R. Agung Susantyoko, Q. Xiao, L. Sun, D. He, Q. Zhang, Nano Energy 5 (2014) 91–96.
[37] J. Zhao, J. Nan, Z. Zhao, N. Li, J. Liu, F. Cui, Appl. Catal. B 202 (2017) 509–517.
[38] M.A.A. Aziz, A.A. Jalil, S. Triwahyono, R.R. Mukti, Y.H. Taufiq-Yap, M.R. Sazegar, Appl. Catal. B 147 (2014) 359–368.
[39] P.R. Ettireddy, N. Ettireddy, S. Mamedov, P. Boolchand, P.G. Smirniotis, Appl. Catal. B 76 (2007) 123–134.
[40] X. Liang, Y. Zang, Y. Xu, X. Tan, W. Hou, L. Wang, Y. Sun, Colloid Surf. A 433 (2013) 122–131.
[41] S. Zhan, H. Zhang, Y. Zhang, Q. Shi, Y. Li, X. Li, Appl. Catal. B 203 (2017) 199–209.
[42] Y.J. Kim, H.J. Kwon, I. Heo, I.S. Nam, B.K. Cho, J.W. Choung, M.S. Cha, G.K. Yeo, Appl. Catal. B 126 (2012) 9–21.
[43] X. Du, C. Li, L. Zhao, J. Zhang, L. Gao, J. Sheng, Y. Yi, J. Chen, G. Zeng, Appl. Catal. B 232 (2018) 37–48.
[44] B. Bai, J. Li, J. Hao, Appl. Catal. B 164 (2015) 241–250.
[45] F. Kapteijn, L. Singoredjo, A. Andreini, Appl. Catal. B 3 (1994) 173–189.
[46] J. Zhong, A. Wang, G. Li, J. Wang, Y. Ou, Y. Tong, J. Mater. Chem. 22 (2012) 5656.
[47] Z. Zhu, G. Lu, Z. Zhang, Y. Guo, Y. Guo, Y. Wang, ACS Catal. 3 (2013) 1154–1164.
[48] S. Ali, L. Chen, Z. Li, T. Zhang, R. Li, Su H. Bakhtiar, X. Leng, F. Yuan, X. Niu, Y. Zhu, Appl. Catal. B 236 (2018) 25–35.
[49] H. Wang, Z. Qu, H. Xie, N. Maeda, L. Miao, Z. Wang, J. Catal. 338 (2016) 56–67.
[50] Z. Hao, Z. Shen, Y. Li, H. Wang, L. Zheng, R. Wang, G. Liu, S. Zhan, Angew. Chem. Int. Ed. 58 (2019) 6351–6356.
[51] Y. Peng, W. Si, X. Li, J. Chen, J. Li, J. Crittenden, J. Hao, Environ. Sci. Technol. 50 (2016) 9576–9582.
[52] Z. Liu, S. Zhang, J. Li, L. Ma, Appl. Catal. B 144 (2014) 90–95.
[53] L. Chen, J. Li, M. Ge, Environ. Sci. Technol. 44 (2010) 9590–9959.
[54] X. Hu, L. Huang, J. Zhang, H. Li, K. Zha, L. Shi, D. Zhang, J. Mater. Chem. A 6 (2018) 2952–2963.
[55] F. Liu, W. Shan, Z. Lian, L. Xie, W. Yang, H. He, Catal. Sci. Technol. 3 (2013) 2699.
[56] J. Liu, X. Li, Q. Zhao, J. Ke, H. Xiao, X. Lv, S. Liu, M. Tadé, S. Wang, Appl. Catal. B 200 (2017) 297–308.
[57] S. Yang, F. Qi, S. Xiong, H. Dang, Y. Liao, P. Wong, J. Li, Appl. Catal. B 181 (2016) 570–580.